

PREPARED FOR SUBMISSION TO JHEP

Dark Matter Induced Nucleon Decay: Model and Signatures

Junwu Huang^a and Yue Zhao^{a,b}

^a*Stanford Institute of Theoretical Physics, Physics Department,
Stanford University, Stanford, CA 94305, USA*

^b*SLAC National Accelerator Laboratory,
2575 Sand Hill Road, Menlo Park, CA 94025, USA*

E-mail: curlyh@stanford.edu, zhaoyue@stanford.edu

ABSTRACT: If dark matter (DM) carries anti-baryon number, a DM particle may annihilate with a nucleon by flipping to anti-DM. Inspired by Hylogenesis models, we introduce a single component DM model where DM is asymmetric and carries B and L as $-1/2$. It can annihilate with a nucleon to an anti-lepton and an anti-DM at leading order or with an additional meson at sub-leading order. Such signals may be observed in proton decay experiments. If DM is captured in the Sun, the DM induced nucleon decay can generate a large flux of anti-neutrinos, which could be observed in neutrino experiments. Furthermore, the anti-DM particle in the final state obtains a relatively large momentum (few hundred MeV), and escapes the Sun. These fast-moving anti-DM particles could also induce interesting signals in various underground experiments.

Contents

1	Introduction	1
2	Model Lagrangian and Parameter choices	4
2.1	Effective operators	4
2.2	UV completion of the Lagrangian	5
3	Choice of parameters	6
4	Relating to Chiral Lagrangian	10
5	Signature searches	12
5.1	Induced Proton Decay in Super-Kamiokande	13
5.2	Signatures from the Sun	15
5.2.1	Dark matter accumulation in the Sun	15
5.2.2	Anti-Neutrino flux from the Sun	16
5.2.3	Anti-DM flux from the Sun	19
6	Conclusion	21
A	DM pair annihilation and elastic scattering	23
B	Dark matter Accumulation: General aspects	24

1 Introduction

Current astrophysical surveys and cosmological studies suggest that dark matter (DM) constitutes about 27% of the energy density of the Universe [1]. The Standard Model (SM) of particle physics cannot explain the abundance of the invisible component. New fundamental physics are required to explain its existence and new experiments are needed to study its nature.

Extensions beyond the standard models contain various weakly interacting massive particles (WIMPs) that are candidates of particle dark matter. In standard WIMP scenarios, the similar magnitude of baryon and DM density, $\Omega_{\text{DM}}/\Omega_B \approx 5.5$ is treated as a numerical coincidence. The baryon asymmetry can be generated from CP-violating non-equilibrium processes (such as the electroweak phase transition), while the DM relic density is determined by thermal freeze out of WIMPs in the early universe. The Asymmetric Dark Matter (ADM) paradigm [4–13], however, provides a framework to relate the baryon and dark matter density.

For a review of Asymmetric Dark Matter models, please see [2] and [3]. Dark Matter in ADM models usually carries a conserved global charge shared by the SM particles, namely, lepton or baryon number. Such a connection naturally relates the number density of DM particles and SM particles. Therefore, the ADM paradigm naturally predicts dark matter particles with a mass of a few GeV. The sensitivity of direct detection experiments drop rapidly if the DM mass is small. New unconventional signatures, if they exist, can help for the DM search.

The existing ADM models generally fall into two classes depending on how the charge asymmetry is created:

- An initial charge asymmetry is first generated in either the visible or DM sector and later transferred to the other sector by chemical equilibration through non-renormalizable operators. The DM in this class of model carry the same baryon/lepton numbers as the left-over SM particles. Such scenario with different variations is recently studied by [12–23].
- Equal and opposite charge asymmetries are generated via non-equilibrium CP-violating dynamics in the visible and DM sectors. The DM in this class of models carries opposite charge baryon/lepton numbers as the left-over SM particles. Such scenario is recently studied by [24–42].

In this paper, we will focus on the second class of models. Very recently, this class of models was re-visited by [40–42] and interesting new experimental signatures were discussed. Let us first review their model. The interaction terms of the Lagrangian of this model is written as follows (here we drop kinematic and mass terms of the particles):

$$\mathcal{L} \supset \frac{\lambda_a}{M^2} \bar{X}_a \bar{d}_R^c \bar{u}_R^c \bar{u}_R^c + \zeta_a \bar{X}_a \Psi^c \Phi^* + h.c. \quad (1.1)$$

where $X_a, X_a^c (a = 1, 2)$ are two vector pairs of hidden sector fermions with masses $m_{X_2} > m_{X_1} \geq \text{TeV}$. Ψ and Φ are two components of the DM relic in their model. There exists a physical CP-violating phase $\arg(\lambda_1^* \lambda_2 \zeta_1 \zeta_2^*)$ that cannot be rotated away through redefinition of the fields.

Baryogenesis begins when a non-thermal, CP- symmetric population of X_1 and \bar{X}_1 is produced in the early Universe. As shown in Fig. 1 these states can decay to SM fields. The interference between the two diagrams gives rise to an asymmetry between the partial widths for $X_1 \rightarrow \bar{u} \bar{d} \bar{d}$ and $\bar{X}_1 \rightarrow u d d$, while the same amount of opposite asymmetry is deposited into DM sector. The amount of asymmetry induced through such interference is estimated as [40]

$$\epsilon = \frac{1}{2\Gamma_{X_1}} [\Gamma(X_1 \rightarrow u d d) - \Gamma(\bar{X}_1 \rightarrow \bar{u} \bar{d} \bar{d})] \simeq \frac{m_{X_1}^5 \text{Im}[\lambda_1^* \lambda_2 \zeta_1 \zeta_2^*]}{256\pi^3 |\zeta_1|^2 M^4 m_{X_2}} \quad (1.2)$$

To achieve successful baryogenesis, one needs to start with a proper reheating temperature. It needs to be high enough to preserve successful nucleosynthesis, while not too high to wash out the asymmetry has already been generated.

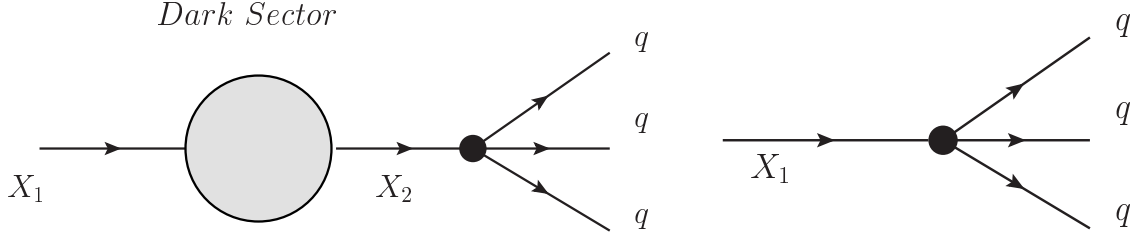


Figure 1. Tree level and one-loop processes that generate an initial baryon asymmetry in the early universe

As suggested in [40–42], interesting signatures could be induced in such models. Since DM particles carry anti-baryon number, they can annihilate visible baryonic matter and produce meson in the final state, i.e. $\Phi + N \rightarrow \bar{\Psi} + M$, where N indicates nucleon and M is meson. Since dark matter particles are invisible, this signal mimics the nucleon decay signatures and offers the possibility to search for dark matter through nucleon decay experiments, e.g. Super-Kamiokande (SuperK) [62]. However, in the model introduced in previous works, two species, one fermion and one boson, of DM are necessary. If the two species of DM particles can decay to each other, then the previously generated baryon asymmetry would be washed out. To avoid such decay, the splitting between their masses needs to be smaller than the sum of proton and electron mass.

In this paper, inspired by the work of [40–42], we present an alternative model which provides similar signatures as induced nucleon decay (IND) processes. The model has the following advantages and features which we will discuss in detail in the following sections:

- We only have one species of dark matter particle, thus no degeneracy between DM masses is required.
- Baryogenesis can be achieved in a similar manner as Hylogenesis. If one assumes zero total baryon/lepton number to start with, we have a concrete prediction on DM mass.
- We have an additional lepton in the final state. This lepton helps to mimic the signatures of proton decay in the best constrained channel. The most sensitive channel in SuperK, $p^+ \rightarrow \pi^0 + e^+$ has the same visible final state particles as $p^+ + \phi \rightarrow \bar{\phi} + \pi^0 + e^+$, leading to a better experimental sensitivity of the IND signals in this model.
- Besides to the 2-to-3 process studied in proton decay experiments, $p^+ + \phi \rightarrow \bar{\phi} + \pi^0 + e^+$, we also have the leading order processes, $p^+ + \phi \rightarrow \bar{\phi} + e^+$ and $n + \phi \rightarrow \bar{\phi} + \bar{\nu}$. These processes have much larger cross section, which can lead to significant anti-DM and anti-neutrino fluxes from the Sun. This can also be studied by underground experiments such as SuperK.

The paper is organized as follows. In Sec. 2, we present our model Lagrangian and study its ultraviolet (UV) completion. In Sec. 3, we discuss constraints on model parameters from

direct detection experiments and collider physics and provide a benchmark set of parameters. In Sec. 4, using the language of chiral Lagrangians, we compute the cross sections of processes that provide interesting experimental signatures. In Sec. 5, we provide a systematic study of three interesting signatures in our model, emphasizing both current constraints and future reaches. Sec. 6 serves as a conclusion.

2 Model Lagrangian and Parameter choices

In this section, we introduce a simple model with one component of dark matter (DM). The DM carries $-\frac{1}{2}$ unit of baryon number and lepton number. DM can annihilate with a proton/neutron to an anti-lepton and an anti-DM in the final state. The baryon and lepton numbers are still conserved in this process. Since the DM/anti-DM in the initial/final state are not detected, such an event fakes a nucleon decay event.

2.1 Effective operators

Let us first write down the effective operators which lead to this induced nucleon decay process. First, since we only introduce one species of DM particle in our model, a DM particle should be in the initial state and an anti-DM is in the final state. Thus we need two copies of DM field in the effective operator. Further, baryon number is changed by one unit in the interaction, to preserve $SU(3)_c$ at the meanwhile, at least three quarks are needed in the operator, and the color indices should be anti-symmetrized. Finally, to preserve Lorentz symmetry, we need one more fermion field in the operator, where the lepton field fits in. To make the operators we write down have the lowest possible dimension, we choose our DM particle to be a scalar field. Following the logic above, one can write down the effective operators ¹

$$\mathcal{O}_S = \frac{1}{\Lambda^4} \bar{\phi}^2 (e^c u^c) (d^c u^c) \quad (2.1)$$

or

$$\mathcal{O}_D = \frac{1}{\Lambda^4} \bar{\phi}^2 (L^\dagger Q^\dagger) (u^c d^c) \quad (2.2)$$

The first operator \mathcal{O}_S only involves $SU(2)_W$ singlet, so only charged lepton shows up in the final state. The second choice, \mathcal{O}_D , can generate either a charged lepton or an anti-neutrino in the final state. This will lead to different signatures to search for.

The operators we write down are dimension 8. One may worry whether one can achieve a sizable signal rate with such high dimension operators. However, this depends highly on the UV model which generates these effective operators. We will address this issue in the rest of this section and show that with a reasonable choice of parameters, various experiments could probe interesting parameter space of this model.

¹There could be other choices, but here we just list two typical ones. The other choices of effective operators will have the similar phenomenology.

2.2 UV completion of the Lagrangian

Now let us go into more detail on how to realize these effective operators. As in to [40–42], we introduce the heavy particle X , and it couples to the quarks through the following effective operators²:

$$\mathcal{O}_{Xq,S} = \frac{1}{\Lambda^2} (Xu^c)(d^c u^c) \quad (2.3)$$

for \mathcal{O}_S , and

$$\mathcal{O}_{Xq,D} = \frac{1}{\Lambda^2} (X^c Q)(u^{c\dagger} d^{c\dagger}) \quad (2.4)$$

for \mathcal{O}_D .³ In both cases, X carries baryon number +1, and zero lepton number. For $\mathcal{O}_{Xq,S}$, X is a $SU(2)_W$ singlet, and for $\mathcal{O}_{Xq,D}$, X is a $SU(2)_W$ doublet. One can introduce multiple generations of X 's. This could lead to physical CP- violating phase and further induce baryogenesis, i.e. Hylogenesis. [40].

To make the connection between DM particle and X , we introduce a gauge singlet scalar field Φ_e . It couples to X and DM particles through the following Lagrangian:

$$\mathcal{L}_{\Phi_e,S} = v\bar{\phi}^2 \Phi_e^* + \lambda_s \Phi_e (X^c e^c) \quad (2.5)$$

for \mathcal{O}_S , and

$$\mathcal{L}_{\Phi_e,D} = v\phi^2 \Phi_e + \lambda_s \Phi_e^* (XL) \quad (2.6)$$

for \mathcal{O}_D . Φ_e is a gauge single, and it carries both baryon and lepton numbers as +1. v is a dimensionful coupling in front of the 3-scalar operator. We will discuss in detail the suitable choices of various parameters in later content.

Now let us summarize the particle content in our model. The DM particle in our model is a scalar. It carries baryon and lepton numbers as $-\frac{1}{2}$. We further introduce X and Φ_e to link DM particle with SM particles. The properties of various particles are summarized in Tab. 2.7.

	$SU(3)_C$	$SU(2)_L$	$U(1)_Y$	$U(1)_L$	$U(1)_B$
X	1	1(2)	1/2	0	1
ϕ	1	1	0	1/2	1/2
Φ_e	1	1	0	1	1

(2.7)

²Here we do not try to UV complete this operator. Detailed discussion can be found in [40–42]. In later section, we will discuss the collider constraint on this operator.

³ To be noticed, similar operators, usually with two X 's, are used in common ADM models, where X is usually taken to be the DM particle.

After integrating out the heavy degree of freedom,⁴ we are left with the following effective operators:

$$\mathcal{L}_{e,S} \supset \frac{\lambda_s v}{\Lambda^2 M_X M_{\Phi_e}^2} \bar{\phi}^2 (e^c u^c) (d^c u^c) \quad (2.8)$$

for \mathcal{O}_S , and

$$\mathcal{L}_{L,\text{eff}} \supset \frac{\lambda_s v}{\Lambda^2 M_X M_{\Phi_e}^2} \bar{\phi}^2 (L^\dagger Q^\dagger) (u^c d^c) \quad (2.9)$$

for \mathcal{O}_D .

Here we want to emphasize that although our effective operators are dimension 8, only Λ and M_X have to be very large due to collider constraints. Φ_e is a gauge singlet. Its mass is barely constrained. Moreover, we have a dimensionful parameter v in the numerator. We will discuss the constraints for each parameter carefully in the next section, and we will see that we could have a sizable interaction cross section with a reasonable choice of parameters.

3 Choice of parameters

In the previous section, we introduce the UV model to the effective operators \mathcal{O}_S and \mathcal{O}_D . In this section, we will focus on the various constraints on parameters, and we choose a benchmark point for the further study.

- DM mass:

As we have discussed in Sec. 1 and Sec. 2, we only focus on the model where DM carries anti-baryon number. If one starts with zero baryon and lepton numbers, DM mass is naturally set to be 2-3 GeV. We will choose DM mass as 3 GeV as a benchmark point. However, baryogenesis is not our focus in this paper. Thus we do not constrain DM mass to be a particular value for various signature studies. DM mass cannot be arbitrarily low. To avoid nucleon decaying to two DM particles, DM mass needs to be larger than 0.5 GeV.

- Dimensionful parameter v :

The dimensionful parameter v can be in principle sizable. However, large v will induce large corrections to scalar masses through the loop diagram. Thus we require the loop corrections to the scalar masses to be smaller than their bare values. This implies $v \lesssim 4\pi \text{ Min}\{m_{\text{DM}}, m_{\Phi_e}\}$.

- Mass of Φ_e :

Φ_e is a gauge singlet. Thus the experimental constraints on its mass is not very strong. However, Φ_e should not be lighter than 1 GeV. It carries both baryon and lepton number. If its mass is smaller than 1 GeV, then the proton can decay to Φ_e and a positron.

⁴In this study, we mainly focus on the DM induced nucleon decay processes. Such processes distribute the nucleon mass, 1 GeV, to the final state particles. The typical 4-momentum in the internal propagators are always smaller than 1 GeV. Thus it is valid to integrate out Φ_e as a heavy particle to generate the effective operator, as long as its mass is larger than nucleon mass.

The mass of Φ_e affects the picture of baryogenesis in our model. If m_{Φ_e} is larger than twice of m_ϕ , then one can directly apply the similar story as Hylogenesis, i.e. the decay of X and \bar{X} induces the asymmetry for both Φ_e and SM sector through interference. When Φ_e later decays to ϕ 's, the asymmetry in Φ_e is transferred into ϕ .

If Φ_e is lighter than twice of m_ϕ , asymmetry in Φ_e cannot propagate to ϕ 's through its decay. Instead, Φ_e will decay to anti-proton and positron caused by the higher dimensional operator. This washes out the asymmetry in SM sector. In this scenario, the asymmetry of DM must be deposited to ϕ through the off-shell Φ_e during X decay. The generated ϕ can annihilate with each other to anti-protons and positrons, i.e. $\phi + \phi \rightarrow \bar{u} + \bar{d} + \bar{d} + e^+$. This is the only process which can wash out the asymmetry in ϕ . However, as long as the reheating temperature is lower than the freeze-out temperature of such wash-out process, the asymmetry of ϕ is not removed.

As we discussed previously, the 3-scalar coupling, v , is chosen to be large, i.e. 4π times the scalar mass scale. Such a large coupling compensates the phase space suppression in the 3-body decay process. Thus the 3-body decay branching ratio of X is comparable to its 2-body decay branching ratio. Then one expects the asymmetry generated when $m_{\Phi_e} < 2m_\phi$ is comparable to the asymmetry when $m_{\Phi_e} > 2m_\phi$. In later discussion, we choose $m_{\Phi_e} = m_\phi = 3$ GeV as our benchmark point.

One may worry whether the decay of Φ_e causes any problems of BBN since its decay lifetime may be long by decaying through the higher dimensional operator. In addition, the reheating temperature needs to be high enough to induce BBN, whether that washes out the asymmetry generated before is another concern. We will cover these subtleties at the end of this section.

- Mass of X and cut-off scale Λ :

X couples to SM particles through two vertices. $\lambda_s \Phi_e (X^c e^c)$ or $\lambda_s \Phi_e^* (XL)$ links X to leptonic sector, and $\frac{1}{\Lambda^2} (Xu^c)(d^c u^c)$ or $\frac{1}{\Lambda^2} (X^c Q)(u^{c\dagger} d^{c\dagger})$ links X to hadronic sector.

Let us first address on the constraints from leptonic sector. Given $\lambda_s \Phi_e (X^c e^c)$ or $\lambda_s \Phi_e^* (XL)$, the strongest constraint comes from the LEP mono-photon search [54–58]. By requiring photon energy larger than 10 GeV, they constrain the product of cross section and acceptance to be smaller than 0.1 pb. This can be reinterpreted into the constraint of our parameters. We study the monophoton channel using MadGraph [68]. As long as $\frac{M_X}{\lambda_s}$ is larger than 0.5 TeV, the model is safe from the LEP constraint.

The other constraint on such operators is muon $(g-2)_\mu$.⁵ Operator $\lambda_s \Phi_e (X^c e^c)$ and $\lambda_s \Phi_e^* (XL)$ can induce large contributions to $(g-2)_\mu$. The corrections to $(g-2)_\mu$ for such models has been calculated and it is summarized in [84]. The leading contribution scales with the mass of particles as

$$\delta a_\mu \simeq \frac{\lambda_s^2}{4\pi^2} \frac{m_\mu^2}{m_{\Phi_e}^2} \frac{m_\mu}{m_X} \quad (3.1)$$

⁵We thank the referee for pointing out this important constraint.

Given the fact that Φ_e is only few GeV, the corrections to $(g-2)_\mu$ can be significant. If we take our benchmark point, i.e. Eq. (3.6), we get $\delta a_\mu \sim 10^{-7}$, which is safely ruled out by the current measurement [85]. However, the precise value of $(g-2)_\mu$ highly depends on the UV model. Especially, the leading contribution under m_X expansion is different by a minus sign when the scalar is a real scalar or a pseudo scalar. To make sure the leading contribution of $(g-2)_\mu$ vanishes precisely, it is crucial to have both $\lambda_s \Phi_e(X^c e^c)$ and $\lambda_s \Phi_e^*(XL)$ operators in our model. The linear combination of these two operators in the Lagrangian should be written as, (here we dropped all the kinematic and mass terms)

$$\mathcal{L} \supset \lambda_s L X_L \Phi_e + \lambda_s e^{\dagger} X_R^{\dagger} \Phi_e^* + h.c. \quad (3.2)$$

Here everything is written in two-spinor convention. L is the SM lepton doublet, and e^c is the right handed lepton. X_L and X_R^c are $SU(2)_W$ doublet and singlet. Given such Lagrangian, $(g-2)_\mu$ correction comes in as the next leading order,

$$\delta a_\mu \simeq \frac{\lambda_s^2}{4\pi^2} \frac{m_\mu^2}{m_{\Phi_e}^2} \frac{m_\mu^2}{m_X^2} \quad (3.3)$$

For our benchmark point, the correction to $(g-2)_\mu$ is very small, $\delta a_\mu \sim 10^{-11}$.⁶ By changing the suppression scales of the operators coupling X_L or X_R^c to quarks can decouple one of X 's in the IND processes. Thus we can and will still treat $\lambda_s \Phi_e(X^c e^c)$ and $\lambda_s \Phi_e^*(XL)$ as two different scenarios in our later discussion for simplicity.

Next we consider the constraint for m_X and Λ from the hadronic side. Here we do not try to UV complete the operator, instead we do a simple parton level analysis and make a conservative choice of parameters. For simplicity, we choose $M_X \sim \Lambda$. A more careful study which includes effects of mediator's width has been carried out in [41], we refer readers to those papers for more details.

For $\frac{1}{\Lambda^2}(Xu^c)(d^c u^c)$, X is an $SU(2)_W$ singlet. Once X is produced through this effective operator, it decays to a charged lepton and DM particles. The signature is 1 jet + l^\pm + MET , where MET is missing transverse energy. For $\frac{1}{\Lambda^2}(X^c Q)(u^{\dagger} d^{\dagger})$, there is also a monojet channel, i.e. 1 jet + MET .

Let us first focus on the monojet channel. This puts constraint on $\frac{1}{\Lambda^2}(X^c Q)(u^{\dagger} d^{\dagger})$, where X decays to neutrinos half of the time. The most recent result on monojet search is from [60]. With a MET cut at 350 GeV⁷, the statistical uncertainty of the monojet cross section is about 4.5 fb. If systematic uncertainties are included, the error bar can only increase. To see how well the monojet search constrain our parameter space, we choose a benchmark point $M_X \sim \Lambda \sim 1$ TeV. Without accounting for the reconstruction efficiency at detector level, only applying the MET cut at parton level already reduces $\sigma \times A$ to 4 fb. A more detailed collider study will only bring $\sigma \times A \times \epsilon$ of our signal lower. Thus we choose $M_X \sim \Lambda \sim 1$ TeV as our conservative benchmark point for further study. To accommodate the LEP constraint, we further choose λ_s as 2 for our benchmark point.

⁶As a side point, one can easily fit $(g-2)_\mu$ anomaly in our model by tuning parameters.

⁷We also checked other values of MET cut, the conclusion does not change.

Now we check the constraint from $1 \text{ jet} + l^\pm + MET$. There is no concrete search optimized for this particular channel so far. If there is b-quark in the final state, the signature is similar to single top production. However, if we take $M_X \sim \Lambda \sim 1 \text{ TeV}$, the parton level cross section for $p + p \rightarrow X + \text{jet}$ is about 30 fb. This is the total cross section for all 3 generations of leptons. Without further event selection and reconstruction, this cross section has already been much smaller than the uncertainty for single top production.

The other channel can be relevant is the W' search. [61] However, this search is optimized for s-channel production. Thus there are 2 kinematic cuts applied to the event selection:

$$\begin{aligned} 0.4 < p_T^l / E_T^{\text{miss}} < 1.5 \\ |\Delta\phi_{l,\text{miss}} - \pi| < 0.2\pi \end{aligned} \quad (3.4)$$

Taking our benchmark value, i.e. $M_X \sim \Lambda \sim 1 \text{ TeV}$, the event selection efficiency for our signal after these two cuts is about 61% at parton level. Assuming flavor universality, the parton level cross section for electron or muon channel after the kinematic cuts is reduced to 2 fb. This is smaller than the constraints from W' search in any mass region. Further, the W' search optimized the M_T^{min} cut with respect to a particular model, which may not be the optimized cut for our signal. Thus our benchmark point is also safe from this search.

To summarize our choice of various parameters, we present our benchmark point as the following:

$$\begin{aligned} m_\phi &= 3 \text{ GeV}, \\ m_{\Phi_e} &= 3 \text{ GeV}, \\ v &= 4\pi m_{\Phi_e} = 3 \times 4\pi \text{ GeV} \\ \lambda_s &= 2, \\ m_X &= \Lambda = 1 \text{ TeV}. \end{aligned} \quad (3.5)$$

Later we will take this benchmark point and estimate signature reaches for various channels. Here we want to emphasize that our benchmark point is a conservative one, and the signal strength could be larger.

Before we end this section, let us demonstrate in a bit more detail some subtleties about the thermal history of our model. First, the reheating temperature cannot be too low for a successful BBN, while it cannot be too high to wash-out the asymmetry through $\phi + \phi \rightarrow \bar{u} + \bar{d} + \bar{d} + e^+$. We calculate the freeze-out temperature for the wash-out process. The annihilation cross section is estimated as

$$\sigma v \simeq \frac{(\lambda_s v)^2}{2048\pi^5} \left(\frac{E^2}{M_X^2 \Lambda^4} \right) \quad (3.6)$$

where E is the typical energy of the process. If we choose the parameters as in the benchmark point, Eq. (3.6), the reheating temperature needs to be smaller than m_ϕ , i.e. $T_{RH} \lesssim m_\phi \sim 3 \text{ GeV}$. Such low reheating temperature is also requested in Hylogenesis models.

At last, we estimate the decay lifetime of Φ_e . Φ_e cannot decay too late, or else it messes up the successful prediction of BBN. The decay lifetime of Φ_e can be easily estimated as

$$\Gamma_{\Phi_e} \sim \frac{\lambda_s^2 m_{\Phi_e}^7}{4096 \pi^5 M_X^2 \Lambda^4} \quad (3.7)$$

Taking the benchmark point in Eq. (3.6), we get the decay lifetime around 10^{-4} s. Thus the decay of Φ_e is also generically safe from BBN constraint.

4 Relating to Chiral Lagrangian

In the previous section, we introduced the effective operators for DM interacting with SM particles at parton level. In this section, we show how the parton level operators are related to nucleons and mesons through chiral Lagrangian. By expanding the chiral Lagrangian in powers of $p_{\text{meson}}/(4\pi f)$, where $f \approx 139$ MeV, one can calculate the cross section for the following processes: $p^+ + \phi \rightarrow e^+ + \bar{\phi}$, $n + \phi \rightarrow \bar{\nu} + \bar{\phi}$ and $p^+ + \phi \rightarrow \pi^0 + e^+ + \bar{\phi}$. These three processes turn out to be the most important processes in the signature searches. In this section, we follow closely [66] for our calculation.

For \mathcal{O}_S and \mathcal{O}_D , the effective Lagrangian after expanding in flavor basis can be written as $\mathcal{L}_{\text{int}} = \sum_i C_i O_i$, where C_i are dimension (-4) constants related to Eq. (2.8) and (2.9). O_i can be written as

$$O_{S1} = \epsilon_{\alpha\beta\gamma} \phi \phi (d_R^\alpha u_R^\beta) (u_R^\gamma e_R) \quad (4.1)$$

$$O_{S2} = \epsilon_{\alpha\beta\gamma} \phi \phi (s_R^\alpha u_R^\beta) (u_R^\gamma e_R) \quad (4.2)$$

$$O_{D1} = \epsilon_{\alpha\beta\gamma} \phi \phi (d_R^\alpha u_R^\beta) (u_L^\gamma e_L - d_L^\gamma \nu_L) \quad (4.3)$$

$$O_{D2} = \epsilon_{\alpha\beta\gamma} \phi \phi (s_R^\alpha u_R^\beta) (u_L^\gamma e_L - d_L^\gamma \nu_L) \quad (4.4)$$

$$O_{D3} = \epsilon_{\alpha\beta\gamma} \phi \phi (d_R^\alpha u_R^\beta) (s_L^\gamma \nu_L) \quad (4.5)$$

α, β, γ are color indices. Here we do not include the operators with two strange quarks since we do not consider final states with two mesons.

The corresponding chiral Lagrangian for \mathcal{O}_S and \mathcal{O}_D is

$$\mathcal{L}_{S,\text{int}} \supset C_{R1} \beta \text{Tr} \left[O \xi^\dagger (B_R e_R) \xi \phi \phi \right] + C_{R2} \beta \text{Tr} \left[\tilde{O} \xi^\dagger (B_R e_R) \xi \phi \phi \right] \quad (4.6)$$

$$\begin{aligned} \mathcal{L}_{D,\text{int}} \supset & C_{L1} \alpha \text{Tr} \left[O \xi (B_L e_L) \xi \phi \phi - O' \xi (B_L \nu_L) \xi \phi \phi \right] \\ & + C_{L2} \alpha \text{Tr} \left[\tilde{O} \xi (B_L e_L) \xi \phi \phi - \tilde{O}' \xi (B_L \nu_L) \xi \phi \phi \right] + C_{L3} \alpha \text{Tr} \left[\tilde{O}'' \xi (B_L \nu_L) \xi \phi \phi \right] \end{aligned} \quad (4.7)$$

where $C_{L,R1} = C_{L,R2} = C_{L3} = \frac{1}{M_s^4}$. For the benchmark point we chose in Eq. (3.6), the suppression scale M_s can be related to the parameters in the Lagrangian by

$$\frac{1}{M_s^4} = \frac{1}{\Lambda^2} \frac{1}{M_X} \lambda_s \frac{v}{m_{\Phi_e}^2} = \frac{1}{(104\text{GeV})^4} \quad (4.8)$$

$B_{L/R}$ is the baryon matrix operator, $\alpha = -0.015\text{GeV}^3$ and $\beta = 0.014\text{GeV}^3$ [67] are the overall constants and $\xi = \exp(iM/f)$ where M is the meson matrix operator.

$$M = \begin{pmatrix} \frac{\eta}{\sqrt{6}} + \frac{\pi^0}{\sqrt{2}} & \pi^+ & K^+ \\ \pi^- & \frac{\eta}{\sqrt{6}} - \frac{\pi^0}{\sqrt{2}} & K^0 \\ K^- & \bar{K}^0 & -\sqrt{\frac{2}{3}}\eta \end{pmatrix}, \quad B = \begin{pmatrix} \frac{\Lambda^0}{\sqrt{6}} + \frac{\Sigma^0}{\sqrt{2}} & \Sigma^+ & p \\ \Sigma^- & \frac{\Lambda^0}{\sqrt{6}} - \frac{\Sigma^0}{\sqrt{2}} & n \\ \Xi^- & \Xi^0 & -\sqrt{\frac{2}{3}}\Lambda^0 \end{pmatrix}. \quad (4.9)$$

The operator O and \tilde{O} are defined in the same way as in [66]

$$O = \begin{pmatrix} 0 & 0 & 0 \\ 0 & 0 & 0 \\ 1 & 0 & 0 \end{pmatrix}, \quad O' = \begin{pmatrix} 0 & 0 & 0 \\ 0 & 0 & 0 \\ 0 & 1 & 0 \end{pmatrix},$$

$$\tilde{O} = -\begin{pmatrix} 0 & 0 & 0 \\ 1 & 0 & 0 \\ 0 & 0 & 0 \end{pmatrix}, \quad \tilde{O}' = -\begin{pmatrix} 0 & 0 & 0 \\ 0 & 1 & 0 \\ 0 & 0 & 0 \end{pmatrix}, \quad \tilde{O}'' = \begin{pmatrix} 0 & 0 & 0 \\ 0 & 0 & 0 \\ 0 & 0 & 1 \end{pmatrix}. \quad (4.10)$$

Now we expand the chiral Lagrangian to leading and next-to leading order, which corresponds to no meson and a single meson respectively in the final state.

For \mathcal{O}_S , the expansion of chiral Lagrangian is given by

$$\mathcal{L}_{\text{int}} \supset C_{R1}\beta p_R e_R \phi \phi - i \frac{C_{R1}\beta}{\sqrt{2}f_\pi} \pi^0 p_R e_R \phi \phi \quad (4.11)$$

and for \mathcal{O}_D ,

$$\mathcal{L}_{\text{int}} \supset C_{L1}\alpha p_L e_L \phi \phi + i \frac{C_{L1}\alpha}{\sqrt{2}f_\pi} \pi^0 p_L e_L \phi \phi \quad (4.12)$$

In this paper, for the single meson channel, we only focus on the pion channel, i.e. $p + \phi \rightarrow \pi^0 + e^+ + \bar{\phi}$. This channel turns out to be the best search channel for SuperK in our later study, see Sec. 5.1.

Here we want to emphasize that the leading processes in our model are 2-to-2 processes, shown as Fig. 2. The only SM particles in the final state is charged lepton or neutrino. Such 2-to-2 processes have much larger cross section comparing to 2-to-3 process. Meanwhile, the 2-to-3 process has more visible particles in the final states, as Fig. 3. This helps to reconstruct the event. These two channels will lead to interesting signatures to look for respectively.

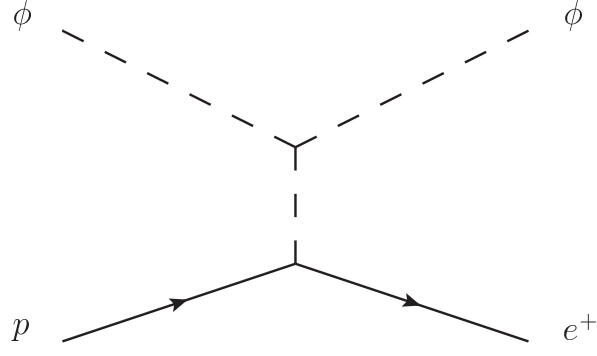


Figure 2. Feynman Diagrams for $p + \phi \rightarrow e^+ + \bar{\phi}$ process in Chiral Perturbation Theory

To get an intuition for the interaction rate for each process, we show the cross section for each process with parameters as our benchmark point, i.e. Eq. 3.6. The cross section for 2-to-2 process is

$$\sigma_{2\text{-to-}2} = 1.87 \times 10^{-43} \text{cm}^2 \quad (4.13)$$

And the cross section of the 2-to-3 process is

$$\sigma_{2\text{-to-}3} = 2.36 \times 10^{-48} \text{cm}^2. \quad (4.14)$$

Given the estimations on the cross sections, in the following section, we will focus on various signatures induced by this model, and we will see how each search channel probes the parameter space.

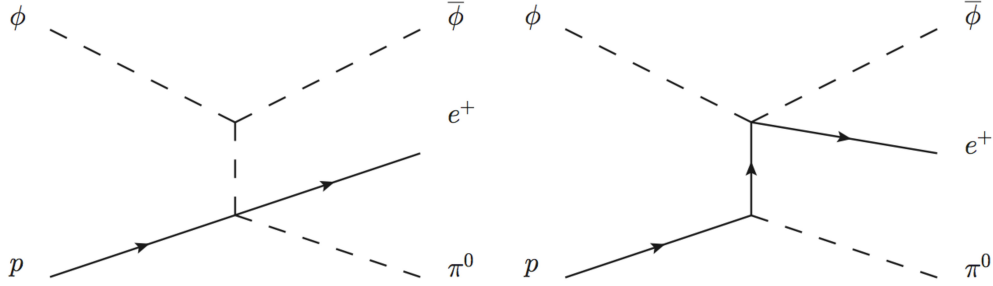


Figure 3. Feynman Diagrams for $p + \phi \rightarrow \pi^0 + e^+ + \bar{\phi}$ process in Chiral Perturbation Theory

5 Signature searches

DM particles annihilating with nucleons could induce several interesting signatures different from ordinary DM search channels. In this section, we focus on the experimental signatures of this model.

First, we will study the signature in proton decay experiment, e.g. Super-Kamiokande, in Sec 5.1. Induced proton decay process has been discussed in the context of magnetic

monopoles in [64, 65]. Similar signatures induced by asymmetric dark matter has also been considered in [40–42]. However, we emphasize that similar signatures in our model have different SM particles in the final states. We benefit from having our signal in the best search channel in proton decay experiments. Also we study in detail on the event selection in such channel, which may further help to improve the search capability.

Furthermore, if DM is captured by the Sun, it can annihilate with the nucleon and may induce a large flux of anti-neutrinos. The neutrino experiments could put strong constraints on such scenario. At last, the anti-DM in the final state is boosted to a high velocity, and it can escape the Sun. Underground experiments may also be able to detect such anti-DM flux from the Sun. We will address each of these signatures in this section.

5.1 Induced Proton Decay in Super-Kamiokande

DM particles in the cosmic background can interact with nucleon in the proton decay experiments and induce signals similar to nucleon decay. Currently, the best nucleon decay experiment is Super-Kamiokande [62], which puts stringent constraints to various nucleon decay channels. In this section, we reinterpret the nucleon decay lifetime limit as a constraint on the DM-nucleon interaction cross section, and study how that constrains the parameter space in our model.

As we have seen in Sec. 4, the dominant annihilation channel between DM and nucleon is through the 2-to-2 process, i.e. $\phi + p^+ \rightarrow \bar{\phi} + e^+$ or $\phi + n \rightarrow \bar{\phi} + \bar{\nu}$. However, such two channels suffer from the large atmospheric neutrino background, which could interact with nucleon through either charge-current or neutral-current interaction. We are forced to consider the next leading processes where one meson is included in the final state.

The most constrained channel in nucleon decay experiments is $p^+ \rightarrow e^+ + \pi^0$. Since we have $\phi + p^+ \rightarrow \bar{\phi} + e^+ + \pi^0$ in the DM-nucleon annihilation process, this channel shares the same visible final states with the best proton decay channel, we will focus on this process and study the implication of the current decay lifetime constraint.

For each proton, the effective decay lifetime can be calculated as the inverse of the interaction rate:

$$\tau_{\text{eff}} = \frac{1}{n_{\text{DM}}(\sigma v)_{\text{IND}}} \quad (5.1)$$

We take the DM energy density around the Earth as $0.3 \frac{\text{GeV}}{\text{cm}^3}$. The annihilation cross section between DM particle and proton for the benchmark point in Eq. (3.6) is $0.707 \times 10^{-40} \text{cm}^3/\text{s}$. Thus the effective proton decay lifetime is

$$\tau_{\text{eff}} = 1.5 \times 10^{33} \text{yr} \left(\frac{0.7 \times 10^{-40} \text{cm}^3/\text{s}}{(\sigma v)_{\text{IND}}} \right) \quad (5.2)$$

A proton lifetime of $1.5 \times 10^{33} \text{yr}$ is shorter compared to the current experimental bound from SuperK for proton decay in this channel ($\tau_p = 8 \times 10^{33} \text{yr}$) [62]. However, this is before

any event selection and reconstruction efficiencies are considered. Since our process is a 2-to-3 scattering process, the kinematics are different from real proton decay. The difference in kinematic distributions can lead to different event selection efficiency. This will further affect the interpretation from the proton decay lifetime to the interaction rate in our model.

For our process, the final state (π^0 and e^+) reconstruction efficiency is the same as proton decay process, since we share the same final state particles within similar energy region. To get rid of the large background from atmospheric neutrinos, SuperK further requests the following two event selection cuts [62]:

- The reconstructed proton's momentum, p_P , needs to be smaller than 250 MeV/ c .
- The reconstructed proton's invariant mass, M_{INV} , needs to be between 800 MeV/ c^2 and 1050 MeV/ c^2 .

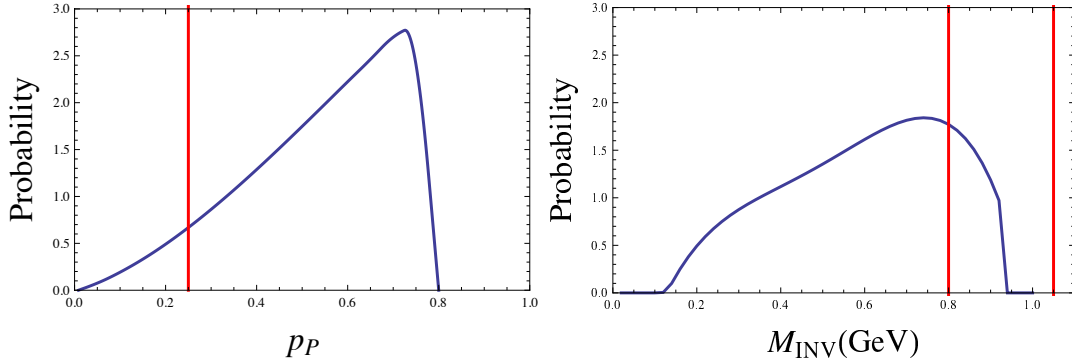


Figure 4. Reconstructed proton transverse momentum and invariant mass cut efficiency of induced nucleon decay searches in SuperK. Red lines in the plots indicate the event selection cuts applied by SuperK.

To estimate the event selection efficiency of these two constraints, we do a MC simulation of our process, as shown in Fig. 4. One can see that the selection efficiency of these two cuts is very low. Only 5.23% of signal events pass the cuts. Taking into account of both final state reconstruction efficiency and event selection efficiency, we get an effective proton decay lifetime of $\tau \simeq 2.9 \times 10^{34} \text{yr}$ for our benchmark point in Eq. (3.6). Such a proton decay lifetime could be reached by Hyper-Kamiokande around 2023. [63] One possibility to improve the experimental reach is to loosen the event selection cuts in a reasonable way. In SuperK analysis, they provide detailed distributions of signal and background on the $M_{\text{INV}} - p_P$ plane [62]. If one loosens the p_P cut from 250MeV/ c to 400MeV/ c , the atmospheric neutrino background are still almost completely removed. However, loosening the cuts in such a mild way can dramatically increase our signal selection efficiency from 5.23% to 20%. This brings the effective proton decay lifetime to $7.5 \times 10^{33} \text{yr}$. Such decay lifetime could have already been probed by SuperK in 2007.⁸

⁸Here we want to emphasize that since we loosen the p_P cut of the event selection, one cannot use the current SuperK reach estimation for a reliable interpretation. To optimize the cuts respect to our signal, a careful study is necessary. However, this is out of the scope of this paper. Here we provide a naive estimation

5.2 Signatures from the Sun

In the previous section, we consider the DM particles in the cosmic background interact with the protons in SuperK. In this section, we consider the possible signatures induced by DM captured in stellar objects. Being asymmetric, DM cannot annihilate with each other. A large number density of DM can exist in the stellar objects. Further, the nucleon number density of the stellar object is usually much higher than matter on the Earth, one expects the IND process happens much more frequently. Here we want to emphasize that in [69–72], one constrains the scalar asymmetric DM models by requiring that the accumulation of DM in neutron star does not cause a black hole in the core. In our model, since DM can annihilate with nucleons, and the anti-DM in the final state of IND process can further annihilate with DM, the accumulation of DM in the neutron star is not efficient enough to form a black hole. Thus the bound is evaded.

Since the Sun has both large DM capture rate and relatively short distance to the Earth, it provides the best place to look for signatures. We will focus on the Sun in the following discussion. For various final states in IND processes, mesons and charged leptons cannot propagate out. To observe such processes on the Earth, we have to rely on the weakly interacting particles, i.e. anti-neutrinos or anti-DM. We first set up the calculation of capture rate and IND interaction rate. Then we will focus on the possible signatures from the anti-neutrino flux in Sec. 5.2.2 and anti-DM flux in Sec. 5.2.3.

5.2.1 Dark matter accumulation in the Sun

In this section, we calculate the accumulation of DM particles in the Sun.⁹ Instead of the IND process, a dark matter particle can also elastically scatter with the hydrogen and helium of the Sun and become captured. The capture rate has been studied by [73]. In Appendix B, we provide a general formula for capture rate. In the range of few GeV DM mass, we can approximate the capture rate to be:

$$C^\odot \simeq 1.3 \times 10^{25} \text{s}^{-1} \left(\frac{\rho_{\text{DM}}}{0.3 \text{GeV/cm}^3} \right) \left(\frac{270 \text{km/s}}{\bar{v}} \right) \left(\frac{1 \text{GeV}}{m_{\text{DM}}} \right) \left(\frac{\sigma_{\text{elas}}}{10^{-40} \text{cm}^2} \right). \quad (5.3)$$

For dark matter mass larger than 10 GeV, an additional kinematic suppression factor needs to be applied.¹⁰ For light DM, the elastic scattering cross section is not strongly constrained by current direct detection experiments. Thus for light DM mass region, we take σ_{elas} to be 10^{-39}cm^2 for spin-independent cross section and 10^{-36}cm^2 for spin-dependent cross section. For large DM mass, we assume the elastic scattering cross section to be the largest value allowed by various direct detection searches.

on the reach capability. This provides an intuition on how much better one can probe the parameter space by optimizing the cuts for the DM induced proton decay process.

⁹A general discussion of the process can be found in Appendix B. We refer the reader to [73, 74, 79] for details.

¹⁰Eq. (5.3) provides a general feeling of the capture rate dependance on the main parameters. The calculations carried in the paper is based on the more accurate equations in Appendix B.

Dark matter particle can thermalize with the Sun after being captured, if DM mass is light, the evaporation from the Sun is not negligible. According to [74], the evaporation rate can be estimated as

$$E^\odot \simeq 10^{-(\frac{7}{2}(m_{\text{DM}}/\text{GeV})+4)} s^{-1} \left(\frac{\sigma_{\text{elas}}}{5 \times 10^{-39} \text{cm}^2} \right) \quad (5.4)$$

Thus one can write the evolution equation for the DM captured in the Sun as

$$\frac{dN_{\text{DM}}}{dt} = C^\odot - N_{\text{Flavor},i}(\sigma v)_{\text{IND}}(\rho_{c,i}/m_i)N_{\text{DM}} - E^\odot N_{\text{DM}}, \quad (5.5)$$

where $(\sigma v)_{\text{IND}}$ is the IND interaction cross section. Unlike in the proton decay search in SuperK, we are looking for the final states of the IND process such as anti-neutrino and anti-DM fluxes. The IND process is dominated by the 2-to-2 scattering channels, i.e. $\phi + p^+ \rightarrow \bar{\phi} + e^+$ and $\phi + n \rightarrow \bar{\phi} + \bar{\nu}$. For our benchmark point, i.e. Eq. (3.6), we get $(\sigma v)_{\text{IND}}$ for the 2-to-2 process as $5.6 \times 10^{-36} \text{cm}^3/\text{s}$. This is a much larger interaction cross section comparing to the 2-to-3 process in SuperK search. $i = n, p$. For \mathcal{O}_S , $N_{\text{Flavor},n} = 0$ and $N_{\text{Flavor},p} = 2$. For \mathcal{O}_D , $N_{\text{Flavor},n} = 3$ and $N_{\text{Flavor},p} = 2$. Since \mathcal{O}_S cannot generate anti-neutrinos in the final state at leading order, we will only focus on \mathcal{O}_D when we discuss anti-neutrino flux in Sec. 5.2.2. On the other hand, both \mathcal{O}_S and \mathcal{O}_D can generate anti-DM flux. In Sec. 5.2.3, we also use \mathcal{O}_D for illustration.¹¹ In Eq. (5.5), we do not include the DM pair annihilation term since the anti-DM produced through IND processes in the Sun will escape the Sun after production, as will be discussed in detail in Sec. 5.2.3. $\rho_{c,i}$ is the mass density of protons and neutrons in the center of the Sun and m_i is the proton and neutron masses. Here we show an illustration on the evolution of ADM number in the Sun for our choice of benchmark point as Fig. 5. We see that the number of ADM approaches a constant at late time due to the equilibrium between capture and IND annihilation.

5.2.2 Anti-Neutrino flux from the Sun

In this section, we focus on the anti-neutrino flux induced by IND process in the Sun. For IND process, DM annihilates with neutrons producing anti-neutrinos in the final state. Neutrons are mainly from helium, which is about 28% mass of the Sun. Since the kinematic energy of the DM particle at the core of the Sun is much smaller than 1 GeV, one can treat the DM particles as at rest for approximation, and then the anti-neutrino from the DM-nucleon annihilation is monochromatic,

$$p_{\bar{\nu}} = \frac{2m_{\text{DM}} + m_{\text{N}}}{2(m_{\text{DM}} + m_{\text{N}})} m_{\text{N}} \quad (5.6)$$

For example, if DM particle mass is 3 GeV, the neutrino in the final state is about 0.88 GeV.

The flux of atmospheric neutrinos has been measured by FREJUS Collaboration [77], the result agrees with the theoretical calculation [75, 76]. Since the neutrino from IND process

¹¹The result from \mathcal{O}_S is only different by an $\mathcal{O}(1)$ factor.

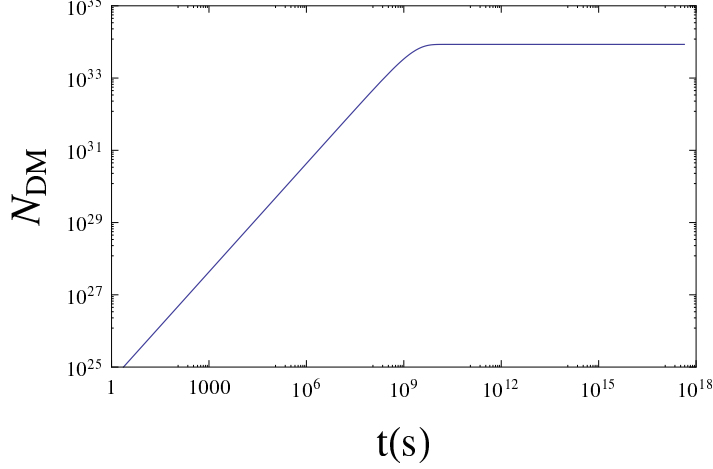


Figure 5. An illustration of the ADM number evolution in the Sun. We choose the parameters according to the benchmark point where the IND cross section is $5.6 \times 10^{-36} \text{cm}^3/\text{s}$. And we take the elastic scattering between DM and nucleons as 10^{-40}cm^2 . One see that the number of ADM approaches a constant at late time due to the equilibrium between capture and IND annihilation.

is monochromatic, we only need to focus on one energy bin of the spectrum. For example, for 0.88 GeV neutrino, the corresponding bin is from 0.76 GeV to 1.00 GeV in FREJUS. The dominant uncertainty is coming from the theoretical uncertainty of the interaction cross section between neutrino and nucleon. Combining all the uncertainties, the error of the bins around 1 GeV is about 22%. By requiring the contribution to neutrino flux from IND process to not exceed 2 sigma error bar, one can constrain the interaction rate of IND process in the Sun.

Note that one can further probe the parameter space of our model by optimizing the neutrino flux measurement. The atmospheric neutrino flux measurement, i.e. [77], does not include the angular information of the neutrino. Since anti-neutrinos from IND process is dominantly from the center of the Sun, the angular information can help to reduce the atmospheric neutrino background dramatically. Furthermore, since the anti-neutrinos from the IND process is monochromatic, a better energy resolution also helps to improve the signal reach. To get an idea on how these improvements may help us probe the parameter space, we quote the energy and angular resolution from the proposal of ICANOE¹² [78]. Since ICANOE is using the information of all particles in the final state, it can achieve a good reconstruction of incoming neutrinos' energy and incidence angle. For the neutrino flux spectrum, energy resolution in ICANOE can be as good as 50 MeV, this is about a factor of 5 improvement comparing to the energy resolution of FREJUS Detector. For neutrinos at around 1 GeV, the angular resolution of the incoming neutrino is about 12 degrees. With the

¹²The ICANOE proposal is based on technology in 1999. With current technology, the resolution may have been improved

angular information, the background can be reduced by a factor of 90. If one fully applies both energy and angular resolution, the number of background events can be reduced dramatically. However, given an exposure of $50 \text{ kton} \times \text{year}$, there will be about 15 events in each bin of fixed energy and incident angle. The statistical uncertainty becomes comparable to the theoretical uncertainty. Thus we take conservative choices of energy and angular resolutions, assuming they can reduce the number of background events by a factor of 200.

To calculate the IND process rate in the Sun, one needs to specify the elastic scattering cross section. This is constrained by various direct detection experiments. For spin independent scattering, when DM mass is larger than 5.5 GeV, the strongest constraint comes from the recent LUX result [45]. Between 3.5 GeV to 5.5 GeV, the CDMS-Lite [43] sets the best constraints. Below 3.5 GeV, there is no constraint. (See [53] for more information.) For the spin dependent case, since the Sun is dominated by protons, we focus on the direct detection constraints for DM-proton elastic scattering. The constraints dominantly come from PICASSO, SIMPLE and COUPP [47–49]. If DM mass is smaller than 4 GeV, the constraints are not strong. To estimate how well the anti-neutrino flux can help to probe our parameter space, we assume the elastic scattering cross section to be just below the constraints from various experiments. When DM mass is too small to be constrained, we take 10^{-39} cm^2 and 10^{-36} cm^2 for spin-independent and spin-dependent cross sections respectively. In Fig. 6, we show the $(\sigma_{\text{IND}} - m_{\text{DM}})$ plane which can be probed by the anti-neutrino flux. The dark blue is the region which is constrained by the current data of atmospheric neutrino flux measurement, assuming the largest elastic scattering cross section allowed by direct detections. The light blue is the region which could be constrained using a better energy resolution and angular information.

From the plot, one can clearly see that the escape rate starts to dominate the loss of the DM particles in the Sun when DM mass is smaller than 4 GeV. If DM particle scatters with nucleon spin-independently, the current neutrino flux measurement cannot probe any interesting parameter space due to the low capture rate. However, if we apply a better energy resolution and angular information as claimed in ICANOE, an interesting region can be probed. The smallest IND cross section can be probed in this scenario is about $3 \times 10^{-43} \text{ cm}^3/\text{s}$, which is corresponding to $m_X \sim \Lambda \sim 24 \text{ TeV}$, assuming all other parameters to be the same as our benchmark point. Further, if the elastic scattering is spin-dependent, the capture rate is much higher, and one can probe a much larger parameter region, both smaller IND cross section and larger DM mass. Using the current measurement, the smallest IND cross section can be probed is about $10^{-45} \text{ cm}^3/\text{s}$, which corresponds to $m_X \sim \Lambda \sim 42 \text{ TeV}$. If we apply the improvements on energy resolution and angular information, one can reach $m_X \sim \Lambda \sim 91 \text{ TeV}$.

On the other hand, if one takes a particular value of the IND cross section, one can constrain the elastic scattering cross section. For example, if we take the benchmark point where the IND cross section is $5.6 \times 10^{-36} \text{ cm}^3/\text{s}$, the constraint on elastic scattering cross section is show as Fig. 7. The constraint for spin-dependent cross section is much stronger than direct detection, while a stronger constraint can only be applied in the lower mass region

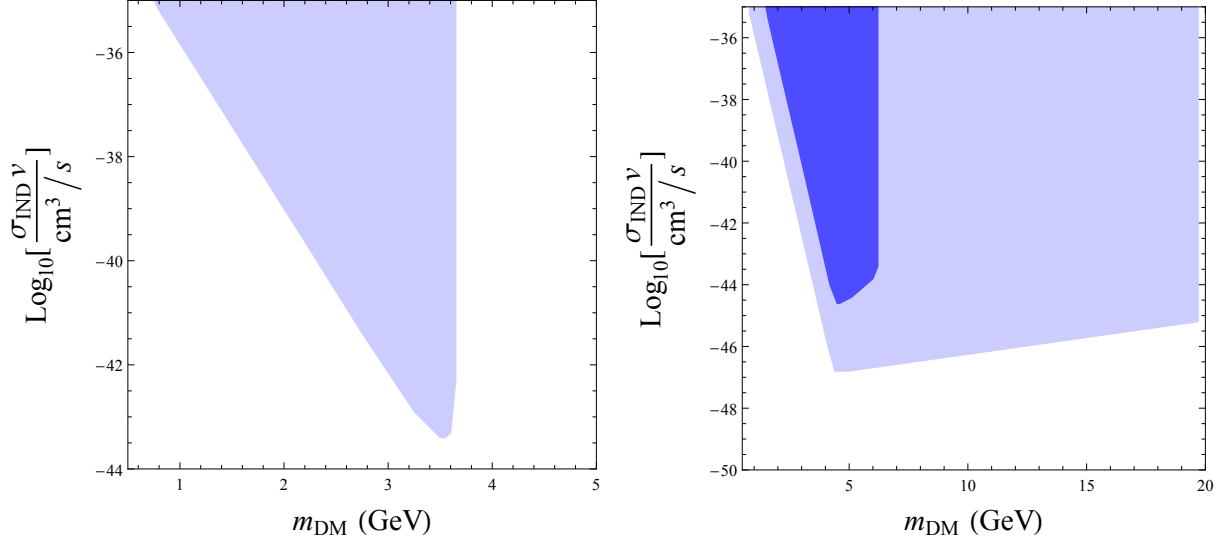


Figure 6. The constraint from neutrino flux on the IND interaction cross section as a function of the DM mass, for Spin-Independent (Left) and Spin-Dependent (Right) elastic scattering respectively. The dark blue region is constrained by the current data. The light blue is the region could be further probed by improving energy resolution and angular information. For spin-independent scattering, the current data of neutrino flux cannot probe any interesting parameter space due to the low capture rate. Taking other parameters the same as our benchmark point, the lowest points in both plots can be interpreted as the cut-off scales, i.e. $m_X \sim \Lambda$. For spin-independent scenario, $\Lambda_{\text{SI,Max}} \sim 24$ TeV, and $\Lambda_{\text{SD,Max}} \sim 91$ TeV for spin-dependent scenario.

for spin-independent elastic scattering.

5.2.3 Anti-DM flux from the Sun

In this section, we discuss another signature in our model, i.e. the anti-DM flux from the Sun. Anti-DM is in the final state of the 2-to-2 induced nucleon decay process, its momentum can be calculated easily by assuming that the initial particles are approximately at rest,

$$p_{\bar{\phi}} = p_l = \frac{2m_{\text{DM}} + m_{\text{N}}}{2(m_{\text{DM}} + m_{\text{N}})} m_{\text{N}} \quad (5.7)$$

For example, if the DM mass is 3 GeV, then the velocity of anti-DM in the final state is about $0.3 c$. This is much larger than the escape velocity. Thus the IND process can generate an anti-DM flux from the Sun. When arriving at the Earth, these fast anti-DM particles can elastically scatter with the nucleus in underground experiment detectors. Due to the large velocity of the anti-DM, it can kick the neutron or proton out of the nucleus. A fast neutron/proton plus a prompt gamma ray from the nucleus de-excitation is the signature of the anti-DM flux.

For a 3 GeV DM particle, the typical velocity of the neutron/proton after the elastic scattering is about $0.4 c \sim 0.5 c$. In SuperK, such proton is not fast enough to generate the

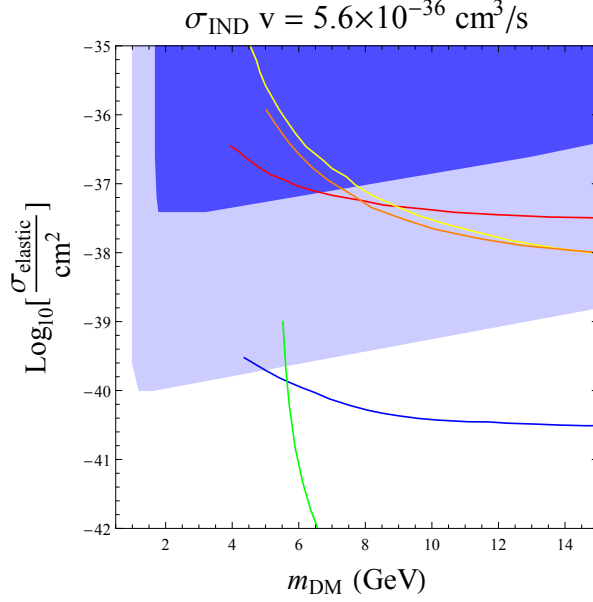


Figure 7. Assuming the IND cross section as our benchmark point, one can constrain the elastic scattering cross section between DM with nucleon. The solid lines are indicating the constraints from direct detections for spin-dependent and spin-independent scattering. The red curve is from PICCASO, orange is from SIMPLE, yellow is from COUPP, Blue is from CDMSlite and Green is from LUX. [43, 45, 47–49]

Cherenkov ring.¹³ Meanwhile, the fast moving neutron can be captured by the hydrogen and release a 2.2 MeV gamma ray. The efficiency for SuperK to see such low energy gamma ray is low, only about 20%. However, if one dopes Gd ion into the water, which is being tested by SuperK, the fast neutron can be captured and releases a gamma ray at about 8 MeV.¹⁴ This could help in triggering our signal. Furthermore, the fast moving proton can leave a long track in the detector since the stopping power is only about $O(1)$ MeV/cm for few hundred MeV proton [81, 82]. A Gd doped liquid scintillator detector, e.g. in Daya Bay experiment [80], though much lighter than SuperK, can provide much more information about the event, such as the incidence energy and angle. This can help to reduce the background efficiently. A detailed study on the experimental details and how to optimize the signal are necessary for the search of this signature, we will leave the details for future study.

A fast-moving proton leaves a long track in material, which is a promise signal on which to trigger. Also there are possibilities to improve the signal with energy and angular information from the proton track, we focus on the signature where the anti-DM knocks out proton from

¹³Here we note that semi-annihilation DM models [86] may also generate fast moving DM flux from the Sun. Therefore, the search proposed in this section can also be applied. The velocity of the DM particle in the final state is model dependent, but generically higher than that of IND process. We will leave the discussion of semi-annihilation models in the future.

¹⁴We gratefully thank Michael Smy and Henry Sobel for very helpful discussions on details about SuperK.

the oxygen nucleus. For current study, we look for the anti-DM flux signature in a conservative way. We assume no knowledge about incidence energy and angle. A much larger parameter region can be probed if one applies the energy and angular information.

We compare the anti-DM flux induced event rate with the indistinguishable background from the neutral-current interaction of the atmospheric neutrino. We account for the neutrino fluxes of all flavors above 100 MeV, since lower energy neutrino will not be able to scatter with an individual nucleon but the whole nucleus of oxygen. By requiring the elastic scattering rate from anti-DM flux to be smaller than $2\text{-}\sigma$ uncertainty of the rate from atmospheric neutrino flux [75, 76], one can constrain the rate of IND process happening in the Sun.

In Fig. 8, we present constraints on the elastic scattering cross section by anti-DM flux from the Sun, assuming the IND interaction cross section as the value of the benchmark point. Here we see that even without energy and angular information, the anti-DM flux provides a reasonable probe of the parameter space. The constraints on SD elastic scattering cross section is better than the constraints from direct detections for a large mass range. It also probes the very light DM mass region which is below the threshold of the direct detections. Here we emphasize that if one apply further energy and angular information from the fast moving proton track, the atmospheric neutrino background can be efficiently reduced, and we will be able to probe much larger parameter space.

Finally, one point needs to be addressed for the detection of the anti-DM flux. All the direct detection constraints on the elastic scattering cross section is derived for the cosmic DM, whose velocity relative to the nucleus is about $10^{-3} c$. However, the anti-DM flux from the Sun has a much larger velocity comparing to the cosmic DM. In the previous study, we assume that the leading order interaction cross section has no velocity dependence. If the elastic scattering cross section between DM and nucleon has non-trivial velocity dependence at leading order, e.g., v^2 ¹⁵, then the fast-moving anti-DM from the Sun could have a much larger scattering cross section than the direct detection bound. However, if the elastic scattering cross section has a strong velocity dependence, anti-DM from the IND process may not be able to leave the Sun without colliding with the nucleons in the Sun. The elastic scattering cross section between the fast moving anti-DM and nucleon is required to be smaller than $8 \times 10^{-37} \text{cm}^2$ in order to escape the Sun. If anti-DM cannot leave the Sun, then it will be trapped and annihilate with the DM particle in the Sun. One can instead constrain the model through the neutrinos in the final state of dark matter pair annihilation. The detailed numbers are model dependent, e.g. the neutrino branching ratio and its energy spectrum, and we refer the reader to [79] for a detailed analysis.

6 Conclusion

In this paper, we study a special scenario of asymmetric dark matter model where DM particle carries anti-baryon and anti-lepton numbers. Our model is inspired by hylogenesis model, [40–

¹⁵The different portals and their constraints are discussed in detail in [83]. The collider bounds on these operators, for example, $\mathcal{O}_{va}^\phi = \frac{1}{\Lambda^2} \phi^\dagger \partial^\mu \phi \bar{f} \gamma_\mu \gamma^5 f$, may be evaded by introducing light mediators

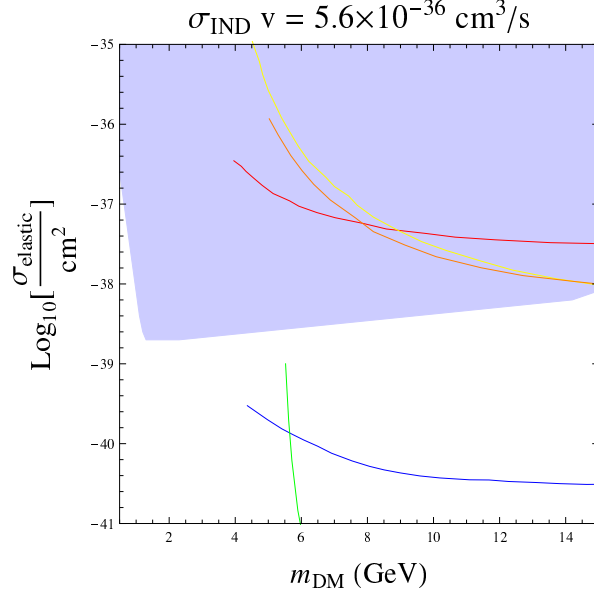


Figure 8. The constraint from anti-DM flux on the elastic scattering cross section between cosmic DM and nucleus as a function of the DM mass. Here we assume the IND interaction cross section to be the value of our benchmark point. The solid lines indicate the constraints from direct detection for spin-dependent and spin-independent scattering. The red curve is from PICCASO, orange is from SIMPLE, yellow is from COUPP, Blue is from CDMSLite and Green is from LUX. [43, 45, 47–49]

[42], but we have several advantages. In original hylogenesis model, there are two species of DM particles, one fermion and one boson. Their masses need to be almost degenerate to avoid the decay between these two species. In our model, we have a similar mechanism to generate baryon asymmetry, but we have only one species of DM particle. Thus our dark matter sector is simpler and no degeneracy is requested. From the signature point of view, we have one lepton in our final state which helps to improve the signature searches.

Since DM particle carries anti-baryon/lepton numbers, they can annihilate with nucleons and induce striking signatures. One of the signatures is the induced proton decay signal in proton decay experiments, such as SuperK. Similar signature also shows up in hylogenesis model. Because of the fact that we can have an additional positron in the final state, our induced proton decay process shares the same SM final states as the most sensitive search channel in SuperK, i.e. $p^+ \rightarrow e^+ + \pi^0$. If we apply the same event selection cuts as what are currently carried in SuperK, one can probe interesting parameter region in very near future. We also give an example on how well one can probe our parameter space by optimizing the event selection cuts respect to our signature. A mild change of cuts improve the sensitivity dramatically, and current SuperK data has already been capable to probe this model.

Further, if DM particles are captured by the Sun, the IND process can induce large anti-neutrino and anti-DM fluxes. The neutrino experiments can be used to study the IND

process rate happening in the Sun by constraining the anti-neutrino flux. This can later be interpreted as parameters in our model. Improving energy and angular resolution of the neutrino experiments can largely enhance the sensitivity. As an illustration, we show how well such information can help us studying our model by a reasonable choice of resolutions according to ICANOE. Finally, anti-DM flux from the Sun can induce similar signature as neutral current interaction between atmospheric neutrinos and nucleons. A conservative estimation is carried out to show how well such signature can be used to probe our parameter space. A more detailed study taking into account the energy and angular information of the fast moving proton in the detector can further improve the sensitivity.

Acknowledgments

We would like to thank Josh Berger, Koun Choi, Savas Dimopoulos, Peter Graham, Giorgio Gratta, Guey-Lin Lin, Jeremy Mardon, Michael Peskin, Surjeet Rajendran, Michael Smy, Henry Sobel, Matt Strassler, Yuhsin Tsai, Sean Tulin and Kathryn Zurek for helpful discussions. This work was supported by ERC grant BSMOXFORD no. 228169 and NSF grant PHY-1316699.

A DM pair annihilation and elastic scattering

In the bulk of the paper, we focus mainly on an ADM model. However, IND processes only rely on the fact that DM carries anti-baryon numbers. In this appendix, we consider the symmetric DM scenario. For IND process in SuperK experiment, the result only changes by a factor of 2, since in the case of symmetric DM, only half of the DM particles can annihilate with nucleons. On the other hand, when calculating the DM accumulation in the Sun, if the DM is symmetric, one has to add the annihilation contribution to the evolution equation.

One may expect that the DM/anti-DM annihilation always dominates over induced nucleon decay process. However, DM/anti-DM annihilation rate is proportional to the product of DM and anti-DM number densities while the IND interaction rate is proportional to the product of DM number density and nucleon number density. Thus the IND process gains a large boost from the enormous nucleon density in the center of the Sun.

As an illustration to this point, we study a symmetric DM scenario with DM mass of 30 GeV. We assume the DM particle scatters with the nucleon through spin-dependent interaction. The elastic scattering cross section is taken to be the largest value allowed by direct detection experiment, i.e. $\sigma_{\text{elastic}} = 3 \times 10^{-38} \text{cm}^2$. Assuming the same energy and angular resolution as stated in 5.2.2 for ICANOE, we study how well the anti-neutrino flux from the Sun can probe the $\sigma_{\text{annihilation}} - \sigma_{\text{IND}}$ plane. The result is shown in Fig. 9.

Here we see that a large region of parameter space can be probed by the IND process induced anti-neutrino flux from the Sun, even for symmetric DM scenario. The red line on the plot is the annihilation cross section which gives the correct relic abundance from a standard thermal history.

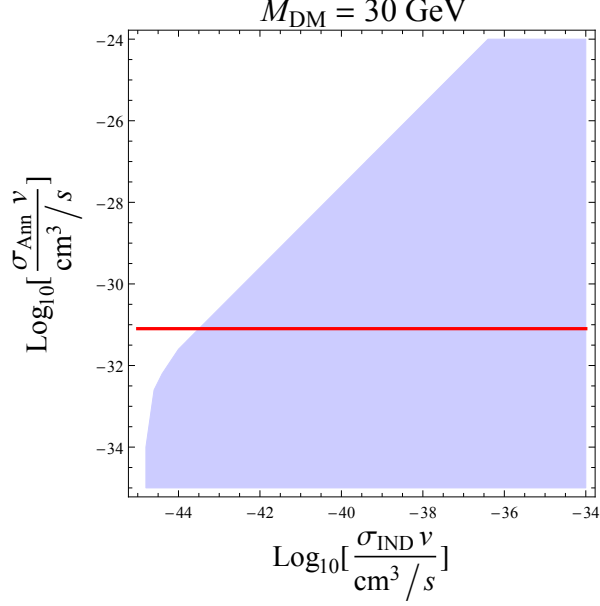


Figure 9. For a symmetric DM scenario with DM mass as 30 GeV, this figure shows how well the anti-neutrino flux from the Sun helps to probe our parameter space. The red line indicates the annihilation cross section to give the correct relic abundance.

B Dark matter Accumulation: General aspects

In this section, we review the general aspects of DM accumulation by stellar objects.

In our model, the DM particles accumulated will be partly converted into its anti-particle by interacting with nucleons in the stellar objects. The total number of dark matter particles ϕ and anti-particles $\bar{\phi}$ can be calculated using:

$$\begin{aligned} \frac{dN_\phi}{dt} &= C_\phi - A_\phi N_\phi N_{\bar{\phi}} - B_\phi N_\phi - E_\phi N_\phi \\ \frac{dN_{\bar{\phi}}}{dt} &= -A_\phi N_\phi N_{\bar{\phi}} + \epsilon_{\bar{\phi}} B_\phi N_\phi - E_{\bar{\phi}} N_{\bar{\phi}} \end{aligned} \quad (\text{B.1})$$

Here, the C_ϕ is the DM capture rates, the A_ϕ describes the DM anti-DM annihilation, the B_ϕ describes DM conversion into anti-DM, while $\epsilon_{\bar{\phi}}$ is the chance that the converted $\bar{\phi}$ is captured by the stellar object. The A_ϕ and B_ϕ can be well approximated by

$$A_\phi \simeq (\sigma v)_{\text{annihilation}} / (4\pi r_{\phi,th}^3/3), \quad (\text{B.2})$$

$$B_i \simeq (\sigma v)_{\text{IND}} (\rho_c/m_n), \quad (\text{B.3})$$

m_n is the mass of the nucleon, and $r_{\phi,th}$ is the thermal radius of the dark matter particles in the stellar objects.

$$r_{\phi,th} = \left(\frac{9T_c}{4\pi G \rho_c m_\phi} \right)^{1/2}, \quad (\text{B.4})$$

ρ_c is the mean baryon density in the center and T_c is center's temperature. In the case of the Sun, the thermal radius for GeV mass DM can be expressed as:

$$r_{\phi,th} \simeq (5 \times 10^9 \text{ cm}) \left(\frac{3\text{GeV}}{m_{\text{DM}}} \right)^{1/2} \left(\frac{T_c}{1.5 \times 10^7 \text{ K}} \right)^{1/2} \left(\frac{1.5 \times 10^5 \text{ kg/m}^3}{\rho_c} \right)^{1/2} \quad (\text{B.5})$$

The capture rate of DM through elastic scattering with nuclei in the Sun can be written as

$$C_\phi \simeq 1.3 \times 10^{25} \text{ s}^{-1} \left(\frac{\rho_{\text{DM}}}{0.3 \text{ GeV/cm}^3} \right) \left(\frac{270 \text{ km/s}}{\bar{v}} \right) \left(\frac{1\text{GeV}}{m_{\text{DM}}} \right) \\ \times \left[\left(\frac{\sigma_{\text{H}}}{10^{-40} \text{ cm}^2} \right) S(m_{\text{DM}}/m_{\text{H}}) + 1.1 \left(\frac{\sigma_{\text{He}}}{16 \times 10^{-40} \text{ cm}^2} \right) S(m_{\text{DM}}/m_{\text{He}}) \right]. \quad (\text{B.6})$$

with \bar{v} being the local dark matter velocity, σ_{H} and σ_{He} are the scattering cross sections between Hydrogen/DM and Helium/DM, respectively. The kinematic suppression function $S(x)$ is defined as:

$$S(x) = \left[\frac{A(x)^{3/2}}{1 + A(x)^{3/2}} \right]^{2/3} \quad (\text{B.7})$$

where

$$A(x) = \frac{3x}{2(x-1)^2} \left(\frac{v_{\text{esc}}}{\bar{v}} \right) \quad (\text{B.8})$$

$v_{\text{esc}} \simeq 617 \text{ km/s}$ is the escape velocity of the Sun.

References

- [1] P. A. R. Ade *et al.* [Planck Collaboration], arXiv:1303.5076 [astro-ph.CO].
- [2] K. M. Zurek, arXiv:1308.0338 [hep-ph].
- [3] K. Petraki and R. R. Volkas, Int. J. Mod. Phys. A **28**, 1330028 (2013) [arXiv:1305.4939 [hep-ph]].
- [4] P. Hut, K. A. Olive, Phys. Lett. **B87**, 144-146 (1979).
- [5] S. Nussinov, Phys. Lett. **B165**, 55 (1985).
- [6] S. Dodelson, L. M. Widrow, Phys. Rev. **D42**, 326-342 (1990).
- [7] G. B. Gelmini, L. J. Hall and M. J. Lin, Nucl. Phys. B **281**, 726 (1987).
- [8] S. M. Barr, R. S. Chivukula, E. Farhi, Phys. Lett. **B241**, 387-391 (1990).

- [9] S. M. Barr, Phys. Rev. **D44**, 3062-3066 (1991).
- [10] D. B. Kaplan, Phys. Rev. Lett. **68**, 741-743 (1992).
- [11] V. A. Kuzmin, Phys. Part. Nucl. **29**, 257-265 (1998). [hep-ph/9701269].
- [12] D. Hooper, J. March-Russell, S. M. West, Phys. Lett. **B605**, 228-236 (2005). [hep-ph/0410114].
- [13] D. E. Kaplan, M. A. Luty, K. M. Zurek, Phys. Rev. **D79**, 115016 (2009). [0901.4117 [hep-ph]].
- [14] G. D. Kribs, T. S. Roy, J. Terning, K. M. Zurek, Phys. Rev. **D81**, 095001 (2010). [0909.2034 [hep-ph]].
- [15] Y. Cai, M. A. Luty and D. E. Kaplan, arXiv:0909.5499 [hep-ph].
- [16] T. Cohen, D. J. Phalen, A. Pierce, K. M. Zurek, Phys. Rev. **D82**, 056001 (2010), [1005.1655 [hep-ph]].
- [17] J. Shelton, K. M. Zurek, Phys. Rev. **D82**, 123512 (2010). [1008.1997 [hep-ph]].
- [18] N. Haba, S. Matsumoto, [1008.2487 [hep-ph]].
- [19] M. Blennow, B. Dasgupta, E. Fernandez-Martinez, N. Rius, JHEP **1103**, 014 (2011), [1009.3159 [hep-ph]].
- [20] J. McDonald, [1009.3227 [hep-ph]].
- [21] B. Dutta, J. Kumar, Phys. Lett. **B699**, 364-367 (2011). [1012.1341 [hep-ph]].
- [22] A. Falkowski, J. T. Ruderman, T. Volansky, JHEP **1105**, 106 (2011), [1101.4936 [hep-ph]].
- [23] M. T. Frandsen, S. Sarkar, K. Schmidt-Hoberg, [1103.4350 [hep-ph]].
- [24] D. H. Oaknin and A. Zhitnitsky, Phys. Rev. D **71** (2005) 023519 [hep-ph/0309086].
- [25] R. Kitano, I. Low, Phys. Rev. **D71**, 023510 (2005). [hep-ph/0411133].
- [26] R. Kitano, I. Low, [hep-ph/0503112].
- [27] G. R. Farrar, G. Zaharijas, Phys. Rev. Lett. **96**, 041302 (2006). [hep-ph/0510079].
- [28] P. -H. Gu, Phys. Lett. **B657**, 103-106 (2007). [0706.1946 [hep-ph]].
- [29] P. -H. Gu, U. Sarkar, X. Zhang, Phys. Rev. **D80**, 076003 (2009). [0906.3103 [hep-ph]].
- [30] H. An, S. -L. Chen, R. N. Mohapatra, Y. Zhang, JHEP **1003**, 124 (2010). [0911.4463 [hep-ph]].
- [31] H. An, S. -L. Chen, R. N. Mohapatra, S. Nussinov, Y. Zhang, Phys. Rev. **D82**, 023533 (2010). [1004.3296 [hep-ph]].
- [32] P. -H. Gu, M. Lindner, U. Sarkar, X. Zhang, [1009.2690 [hep-ph]].
- [33] L. J. Hall, J. March-Russell, S. M. West, [1010.0245 [hep-ph]].
- [34] J. J. Heckman, S. -J. Rey, [1102.5346 [hep-th]].
- [35] D. E. Kaplan, G. Z. Krnjaic, K. R. Rehermann, C. M. Wells, [1105.2073 [hep-ph]].
- [36] N. F. Bell, K. Petraki, I. M. Shoemaker, R. R. Volkas, [1105.3730 [hep-ph]].
- [37] C. Cheung, K. M. Zurek, [1105.4612 [hep-ph]].
- [38] J. March-Russell and M. McCullough, JCAP **1203**, 019 (2012) [arXiv:1106.4319 [hep-ph]].
- [39] M. L. Graesser, I. M. Shoemaker and L. Vecchi, arXiv:1107.2666 [hep-ph].

- [40] H. Davoudiasl, D. E. Morrissey, K. Sigurdson and S. Tulin, Phys. Rev. Lett. **105**, 211304 (2010) [arXiv:1008.2399 [hep-ph]].
- [41] H. Davoudiasl, D. E. Morrissey, K. Sigurdson and S. Tulin, Phys. Rev. D **84**, 096008 (2011) [arXiv:1106.4320 [hep-ph]].
- [42] N. Blinov, D. E. Morrissey, K. Sigurdson and S. Tulin, Phys. Rev. D **86**, 095021 (2012) [arXiv:1206.3304 [hep-ph]].
- [43] R. Agnese, A. J. Anderson, M. Asai, D. Balakishiyeva, R. B. Thakur, D. A. Bauer, J. Billard and A. Borgland *et al.*, arXiv:1309.3259 [physics.ins-det].
- [44] R. Agnese *et al.* [CDMS Collaboration], [arXiv:1304.4279 [hep-ex]].
- [45] D. S. Akerib *et al.* [LUX Collaboration], arXiv:1310.8214 [astro-ph.CO].
- [46] C. E. Aalseth *et al.* [CoGeNT Collaboration], Phys. Rev. Lett. **106**, 131301 (2011) [arXiv:1002.4703 [astro-ph.CO]].
- [47] S. Archambault *et al.* [PICASSO Collaboration], Phys. Lett. B **711**, 153 (2012) [arXiv:1202.1240 [hep-ex]].
- [48] M. Felizardo, T. Morlat, A. C. Fernandes, T. A. Girard, J. G. Marques, A. R. Ramos, M. Augste and D. Boyer *et al.*, Phys. Rev. Lett. **105**, 211301 (2010) [arXiv:1003.2987 [astro-ph.CO]].
- [49] E. Behnke *et al.* [COUPP Collaboration], Phys. Rev. D **86**, 052001 (2012) [arXiv:1204.3094 [astro-ph.CO]].
- [50] E. Aprile *et al.* [XENON100 Collaboration], Phys. Rev. Lett. **111**, 021301 (2013) [arXiv:1301.6620 [astro-ph.CO]].
- [51] E. Aprile *et al.* [XENON100 Collaboration], Phys. Rev. Lett. **109**, 181301 (2012) [arXiv:1207.5988 [astro-ph.CO]].
- [52] G. Angloher, M. Bauer, I. Bavykina, A. Bento, C. Bucci, C. Ciemniak, G. Deuter and F. von Feilitzsch *et al.*, Eur. Phys. J. C **72**, 1971 (2012) [arXiv:1109.0702 [astro-ph.CO]].
- [53] A. Kusenko and L. J. Rosenberg, arXiv:1310.8642 [hep-ph].
- [54] P. J. Fox, R. Harnik, J. Kopp and Y. Tsai, Phys. Rev. D **84**, 014028 (2011) [arXiv:1103.0240 [hep-ph]].
- [55] P. Achard *et al.* [L3 Collaboration], Phys. Lett. B **587**, 16 (2004) [hep-ex/0402002].
- [56] J. Abdallah *et al.* [DELPHI Collaboration], Eur. Phys. J. C **38**, 395 (2005) [hep-ex/0406019].
- [57] A. Heister *et al.* [ALEPH Collaboration], Eur. Phys. J. C **28**, 1 (2003).
- [58] G. Abbiendi *et al.* [OPAL Collaboration], Eur. Phys. J. C **18**, 253 (2000) [hep-ex/0005002].
- [59] [ATLAS Collaboration], ATLAS-CONF-2012-147.
- [60] [CMS Collaboration], CMS-PAS-EXO-12-048.
- [61] [ATLAS Collaboration], ATLAS-CONF-2012-132.
- [62] H. Nishino *et al.* [Super-Kamiokande Collaboration], Phys. Rev. D **85**, 112001 (2012) [arXiv:1203.4030 [hep-ex]].

- [63] K. Abe, T. Abe, H. Aihara, Y. Fukuda, Y. Hayato, K. Huang, A. K. Ichikawa and M. Ikeda *et al.*, arXiv:1109.3262 [hep-ex].
- [64] S. Dimopoulos, S. L. Glashow, E. M. Purcell and F. Wilczek, *Nature* **298**, 824 (1982).
- [65] S. Dimopoulos, J. Preskill and F. Wilczek, *Phys. Lett. B* **119**, 320 (1982).
- [66] M. Claudson, M. B. Wise and L. J. Hall, *Nucl. Phys. B* **195**, 297 (1982).
- [67] S. Aoki *et al.* [JLQCD Collaboration], *Phys. Rev. D* **D62**, 014506 (2000). [hep-lat/9911026].
- [68] J. Alwall, M. Herquet, F. Maltoni, O. Mattelaer and T. Stelzer, *JHEP* **1106**, 128 (2011) [arXiv:1106.0522 [hep-ph]].
- [69] S. D. McDermott, H. -B. Yu and K. M. Zurek, *Phys. Rev. D* **85**, 023519 (2012) [arXiv:1103.5472 [hep-ph]].
- [70] I. Goldman and S. Nussinov, *Phys. Rev. D* **40**, 3221 (1989).
- [71] A. Gould, B. T. Draine, R. W. Romani and S. Nussinov, *Phys. Lett. B* **238**, 337 (1990).
- [72] B. Bertoni, A. E. Nelson and S. Reddy, arXiv:1309.1721 [hep-ph].
- [73] A. Gould, *Astrophys. J.* **388**, 338 (1991)
- [74] K. Griest and D. Seckel, *Nucl. Phys. B* **283**, 681 (1987) [Erratum-ibid. B **296**, 1034 (1988)].
- [75] M. Honda, T. Kajita, K. Kasahara, S. Midorikawa and T. Sanuki, *Phys. Rev. D* **75**, 043006 (2007) [astro-ph/0611418].
- [76] M. Honda, T. Kajita, K. Kasahara and S. Midorikawa, *Phys. Rev. D* **83**, 123001 (2011) [arXiv:1102.2688 [astro-ph.HE]].
- [77] W. Rhode *et al.* [Frejus Collaboration], *Astropart. Phys.* **4**, 217 (1996).
- [78] F. Cavanna *et al.* [ICANOE Collaboration], LNGS-P21-99-ADD-2.
- [79] D. Hooper, F. Petriello, K. M. Zurek and M. Kamionkowski, *Phys. Rev. D* **79**, 015010 (2009) [arXiv:0808.2464 [hep-ph]].
- [80] X. Guo *et al.* [Daya-Bay Collaboration], hep-ex/0701029.
- [81] M. J. Berger, J. S. Coursey, and M. A. Zucker, National Institute of Standards and Technology (see <http://physics.nist.gov/PhysRefData/Star/Text/contents.html>) (2000)
- [82] S. Agostinelli *et al.* [GEANT4 Collaboration], *Nucl. Instrum. Meth. A* **506**, 250 (2003).
- [83] J. March-Russell, J. Unwin and S. M. West, *JHEP* **1208**, 029 (2012) [arXiv:1203.4854 [hep-ph]].
- [84] F. Jegerlehner and A. Nyffeler, *Phys. Rept.* **477**, 1 (2009) [arXiv:0902.3360 [hep-ph]].
- [85] D. Hanneke, S. F. Hoogerheide and G. Gabrielse, arXiv:1009.4831 [physics.atom-ph].
- [86] F. D’Eramo and J. Thaler, *JHEP* **1006**, 109 (2010) [arXiv:1003.5912 [hep-ph]].